

3.5.1: Number of functional MoUs/linkages

LINKAGE

**Yashwantrao Chavan Warana Mahavidyalaya,
Warananagar, Dist.-Kolhapur**



and

K.R.P. Kanya Mahavidyalaya, Islampur, Dist.-Sangali



Linkage is signed on 1st July 2018 between

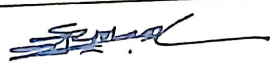
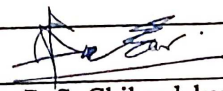
1. Yashwantrao Chavan Warana Mahavidyalaya, Warananagar - First Party.
and
2. Department of Chemistry, K.R.P. Kanya Mahavidyalaya, Islampur-
Second Party.

It is agreed by the First party and Second party to impart sharing of human resources and infrastructure for research to the students. Both the parties have discussed in detail the areas of co-operation and mutually agreed to make the linkage. Now it has been agreed by and between both the parties with the following terms and conditions.

Terms and Conditions:

- 1) Both the parties will extend their facilities to each other in the areas of research, research publications to the students.
- 2) No rental charges or any other incidental charges, unless mentioned, shall be paid by both the parties for using the infrastructure facilities of each other.
- 3) The research contents developed jointly will be published as a joint publication.
- 4) The IPR and patents produced out of the linkage will have equal rights of both the parties mentioned above

- 4) The IPR and patents produced out of the linkage will have equal rights of both the parties mentioned above.
- 5) The linkage will be valid for a period of **five years** starting from the date of signing this agreement and may be renewed for a further period of **five years** through mutual consent of parties.
- 6) This linkage may be terminated by either side by giving three months' notice to that effect in writing.
- In witness where of, the parties here have set these hands on the 1st July, 2018.

Party	First Party	Second Party
Institute	Yashwantrao Chavan Warana Mahavidyalaya, Warananagar, Dist.-Kolhapur	Smt. K. R. P. Kanya Mahavidyalaya, Islampur, Dist. - Sangli
Signature		
Name & Designation	Dr. B. S. Shirke Department of Chemistry	Dr. S. R. Mane Associate Prof. Department of Chemistry
Signature		
Name and designation	Prof. Dr. P. S. Chikurdekar I/C Principal	Dr. Vilas. G. Kale Principal
Stamp	PRINCIPAL Yashwantrao Chavan Warana Mahavidyalaya Warananagar, Dist. Kolhapur.	PRINCIPAL Smt. Kusumtal Rajarambapu Patil Kanya Mahavidyalaya, Islampur Tal. Walwa, Dist. Sangli
Seal		



ISSN: 0976-3031

Available Online at <http://www.recentscientific.com>

CODEN: IJRSFP (USA)

International Journal of Recent Scientific Research
Vol. 11, Issue, 05(C), pp. 38560-38567, May, 2020

**International Journal of
Recent Scientific
Research**

DOI: 10.24327/IJRSR

Research Article

THE LPG GAS-SENSING PERFORMANCE OF $\text{CeO}_2\text{-CuO}$ NANOCOMPOSITE FILM SYNTHESIZED BY MICROWAVE ASSISTED SOL-GEL METHOD

¹Kabure A. A., ²Mane S. R., and ^{1*}Shirke B. S.

^{1*}Material Science Laboratory, Department of Chemistry, Y. C. Warana Mahavidyalaya, Warananagar, India

²Department of Chemistry, K. R. P. Kanya Mahavidyalaya, Islampur, India

DOI: <http://dx.doi.org/10.24327/ijrsr.2020.1105.5335>

ARTICLE INFO

Article History:

Received 6th February, 2020

Received in revised form 15th March, 2020

Accepted 12th April, 2020

Published online 28th May, 2020

Key Words:

CeO_2 , Nanocomposites, HRTEM, SEM, X-Ray Diffraction, LPG, Gas Sensor

ABSTRACT

High demand of semiconductor gas sensors works at low operating temperature has led to the fabrication of gas sensor based on CeO_2 nanoparticles. The aim of the work was to obtain $\text{CeO}_2\text{-CuO}$ nanocomposites with heightened surface area by a simple microwave assisted sol-gel method and to study gas sensing properties towards propane-butane mixture (LPG). The morphological and structural properties of the sensing film were characterized by X-Ray Diffraction (XRD), Transmission Electron Microscope (TEM), Scanning Electron Microscope (SEM) and UV-Visible spectroscopy technique. A $\text{CeO}_2\text{-CuO}$ nanocomposite has a well-defined cubic structure with a crystallite size of ~ 10 nm. Spherical shapes of the as prepared nanocomposite were observed under HRTEM. The SEM image of $\text{CeO}_2\text{-CuO}$ nanocomposite displays spongy-like features with large voids and small spherical agglomerates of CuO, which is useful in gas sensing application. It is found that the $\text{CeO}_2\text{-CuO}$ system includes CeO_2 surface sites with oxygen vacancies for oxygen sorption. The XRD patterns of composite samples revealed distinct peaks of CeO_2 and CuO, which clearly indicates formation of $\text{CeO}_2\text{-CuO}$ nanocomposites. An optical analysis shows the lowering of band gap energy from 3.19 eV ($E_g\text{-CeO}_2$), 1.7 eV ($E_g\text{-CuO}$) to 1.3 eV ($E_g\text{-CeO}_2\text{-CuO}$). The gas sensing behavior of the pure and composite sensor was systematically investigated for the target gas LPG. Under optimum operating temperature of 275°C and 24 ppm LPG, the $\text{CeO}_2\text{-CuO}$ sensor showed maximum response of 57.09%. The response and recovery time of $\text{CeO}_2\text{-CuO}$ sensor for LPG was found to be ~ 25 s and ~ 50 s, respectively. The $\text{CeO}_2\text{-CuO}$ sensor showed better response than pure CeO_2 and CuO sensor, which is attributed to n-p heterojunction at the intergrain boundaries.

Copyright © Kabure A. A., Dr Mane S. R., and Dr Shirke B. S., 2020, this is an open-access article distributed under the terms of the Creative Commons Attribution License, which permits unrestricted use, distribution and reproduction in any medium, provided the original work is properly cited.

INTRODUCTION

This work is the beginning stage in our investigation of gas sensor properties regarding LPG of different $\text{CeO}_2\text{-CuO}$ structures obtained by microwave assisted sol-gel method. There are different methods for the synthesis of ceria nanocomposite such as solvothermal synthesis, thermal decomposition, microwave assisted sol-gel, solution precipitation, hydrothermal crystallization, mechanochemical, sol-gel and thermal hydrolysis [1, 2, 3]. But, microwave assisted sol-gel method has advantages like consequent dramatic increase in reaction rate, high reaction yields, reaction selectivity, and ease of handling. Here, heating arises from dipole rotation or ion migration, which then produce fast homogeneous nucleation and easy gel dissolution [1]. Microwave synthesis of metal oxide nanoparticles is simple, economic, selective process, consumes less energy and fast production speed with

better quality [4, 5]. Ceria and ceria-based oxide materials are the functional rare-earth oxides for their wide applications in gas sensing, environmental chemistry, catalysts, solid oxide fuel cells (SOFC), oxygen membranes, metal-oxide semiconductor devices. The morphology and nanostructure are two essential factors in the functional performance of ceria and ceria-based oxide materials [6]. Nanocrystalline and porous CeO_2 offer high affinity for the development of lots of oxygen vacancies due to the practical redox potential of Ce and the ability to maintain the electro neutrality of the Ce and O species. The consolidation of a foreign metal, for example, lanthanide or transition metals onto the CeO_2 lattice can change its chemical and electronic properties and is therefore expected to advance the redox properties of CeO_2 in the final metal/oxide composition, which leads to higher oxygen mobility [7]. Nanocrystalline Cu-based materials have been indicated remarkable execution in gas-phase

*Corresponding author: Dr Shirke B. S

Material Science Laboratory, Department of Chemistry, Y. C. Warana Mahavidyalaya, Warananagar, India

reactions. Hence, CuO is chosen for sensing application which has unique properties like high specific surface area, chemical stability, electrochemical activity, high electron communication features [8]. The fundamental concern right now is focused particularly on the surface conductive metal oxide gas sensors. The main feature of conductometric semiconducting metal oxide gas sensors is reversible interaction of the gas with the surface of the material [9]. Specifically, the composite of copper oxides (CuO) and cerium oxide (CeO₂) is of great interest because of their catalytic and redox activities [10, 11]. A few examinations on Ce-Cu-O frameworks have recommended that change in the oxidation state of both Ce and Cu in ceria-copper framework; can promote the rate of reaction at the metal oxide interface [12-15]. Such a redox mechanism is succeeded by the formation of a Cu¹⁺ species (Cu²⁺ ↔ Cu¹⁺) in CuO, which is related with the reduction of adjacent CeO₂ (Ce⁴⁺ ↔ Ce³⁺) [16]. The activity of CuO/CeO₂ catalysts is related to the highly dispersed CuO species, its strong interaction with CeO₂, and mutual effect between Cu^{1+/2+} and Ce^{3+/4+} redox couples [17]. The multi valence state of cerium leads to remarkable properties of the material such as oxygen storage and releasing capacity [18, 19]. The large surface area to volume ratio existing in a nanoparticle allows CeO₂ to react differently resulting in unique properties [8, 20]. It is notable that, the dispersion and valence state of copper species, solid solution, and oxygen vacancies associated with the synergistic interaction and catalytic performance rely on the preparation methods [10]. For example, Wang *et al.* [21] reported that, the solvent-free method facilitated the formation of synergistic interaction between copper species and ceria to result in smaller crystallite size and the formation of more Cu⁺ species together with a high ratio of Ce³⁺. Shang *et al.* [22] showed that, the impregnation method offered highly dispersed CuO and stronger synergistic interaction between CuO and CeO₂ to promote the reduction of CuO to Cu⁺ species at the Ce-Cu interface, resulting in the highest catalytic activity. Highly sensitive gas detecting devices has expanding demand in several applications. An effective strategy to improve sensor execution is to embrace the nanostructured sensing materials that have a high surface area to volume ratio and consequently a strong interaction arises between the surrounding gas and the material [23]. Presently, liquefied petroleum gas (LPG) is an energizing option in contrast to regular energy sources, because of its abundance and low cost [24]. The LPG is a combustible blend of hydrocarbon gases used as fuel in many applications like industries, homes, vehicles, hostels, automobiles on account of its attractive properties which incorporate high calorific value, less smoke, virtual lack of sulphur; which brings about clean burning and less harm to the environment [25]. Among various gases, the probability to control propane-butane mixture (LPG) content in air is of high importance due to its high explosiveness [26]. Sensitivity has been drawing in more consideration, as one of the significant parameters of gas sensors and much exertion has been made to improve the sensitivity of gas sensors. The authors have proved that the increase in the temperature up

to a certain value leads to heightening in the sensitivity. On the other hand, the further temperature growth results in the decrease in the sensor sensitivity. Thus, there is an optimum temperature value corresponding to the maximum sensitivity of the sample. The objective of this study is to determine the ideal method and technological parameters corresponding to formation of material with the highest sensor response.

Experimental

Materials and chemicals

All the chemicals used for the preparation were of analytical grade. It includes cerium nitrate [Ce(NO₃)₃.6H₂O] (99%), copper chloride [CuCl₂.2H₂O] (99%), propylene glycol [C₃H₈O₂] and ammonia. All the solutions were prepared in distilled water.

Synthesis of nanocomposite material

The CeO₂ powder was prepared by the microwave assisted sol-gel method. All the chemical reagents used without further purification. Cerium nitrate and propylene glycol were used as starting precursors. Mixture of 0.1M aqueous solution of cerium nitrate and propylene glycol was prepared with ratio of concentration 1:1. The CeO₂ metal oxide powder preparation was achieved with dropwise addition of aqueous ammonia [NH₄OH] to the above mixture with constant stirring. The addition of aqueous ammonia was continued until the solution reached pH = 10. After complete gel formation, that gel hydroxide was washed with distilled water. Then pure hydroxide in a glass beaker was placed in a microwave oven (in put power 600W) for about 30 minutes with on-off cycle. The obtained oxide sample was crushed to prepare fine powder. In the same way, CuO powder was prepared by using copper chloride. For the synthesis of CeO₂-CuO composite, same procedure was followed, by mixing solution of copper chloride and cerium nitrate.

Fabrication of the sensing film

The paste of CeO₂-CuO nanocomposite was prepared by mixing the resulting CeO₂-CuO nanopowder with a temporary binder as a mixture of organic solvent. The ratio of inorganic to organic part was kept as 80:20 in formulating the paste. The paste was then used to prepare thin films on substrate in desired pattern of size (4 mm × 9 mm) by screen-printing technique. These films were dried and cured at 80°C, followed by firing at 200°C for 30 min in air ambient atmosphere. Silver contacts were made by vacuum evaporation for gas sensing measurements. The sensing performance of the sensors was examined using a static gas sensing system. There are electrical feeds on the base plate, a heater was fixed on the base plate. The sample under test was mounted above the heater. A Cr-Al thermocouple was mounted on the heater to measure the operating temperature of the sensor. The required gas concentration inside the static system was achieved by injecting a known volume of test gas by a gas-injecting syringe. A constant 10 V d.c. voltage was applied to the thin film of CeO₂-CuO and current was measured by a

multimeter. The air was allowed to pass into the glass dome after every LPG gas exposure cycle.

Characterization of nanocomposite material

The X-ray diffraction of the powder samples were measured on 'Rigaku Miniflex 600' diffractometer with Cu-K α radiation ($\lambda=1.5405\text{\AA}$) operating at 45 kV and 100 mA over a range of 2θ angle from 10° to 80° , at a scanning rate of $5^\circ/\text{min}$. HRTEM study of the powder sample was carried out by using model number JEE-2100, (JEOL) 200KV (SAIF-NEHU, Shillong). The surface morphology of the films was analyzed using a SEM [scanning electron microscope model JEOL 6300 (LA) Germany]. The UV-Visible (UV-Vis) absorption spectra were recorded in a 'Jasco (model V-770) UV-Vis-NIR Spectrophotometer' in the wavelength range 200 to 800 nm.

RESULTS AND DISCUSSION

X-Ray Diffraction (XRD) analysis

Crystalline structures of all materials were identified by X-ray diffraction. Figure 1.1 shows XRD patterns of pure CeO $_2$, pure CuO and CeO $_2$ -CuO nanocomposite. The

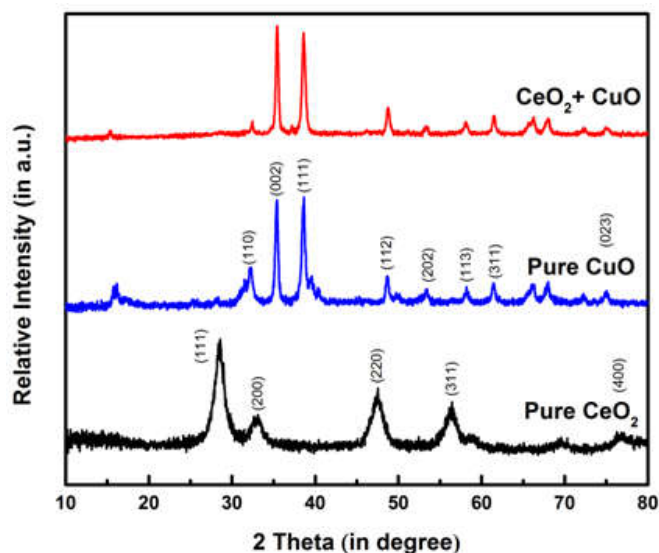


Figure 1.1 XRD patterns of CeO $_2$, CuO nanoparticles and CeO $_2$ -CuO Nanocomposite

XRD peaks of CeO $_2$ at 2θ of 28.6° , 33.1° , 47.3° , 56.5° , 77.2° were respectively indexed as (111), (200), (220), (311), (400) planes of face centered cubic structure (FCC) structure according to (JCPDS file no. 081-0792) and lattice parameter is 5.42\AA [27]. The average crystallite size of the synthesized samples was calculated using Scherrer's formula-

$$d = 0.9 \lambda / \beta \cos\theta, \quad \text{--- eq. (1)}$$

where d is average crystallite size, λ is wavelength of Cu-K α radiation (1.5406\AA), β is full width at half maximum (FWHM) and θ is Bragg's angle. It is seen from XRD that average crystallite size of CeO $_2$ was found to be 26 nm. The XRD spectrum exhibits an intense peak for (111) plane. The diffraction peaks of pure CuO at 2θ of 32.2° , 35.4° , 38.6° , 48.6° , 53.4° , 58.1° , 61.5° , 75.0° were respectively indexed as (110), (002), (111), (112), (202),

(113), (311), (023) planes which are in good agreement with CuO powder file (JCPDS no.80-1917) which corresponds to the monoclinic structure [28]. Further, no other impurity peak was observed in the XRD pattern, showing the single phase sample formation. It is seen from XRD that average crystallite size of CuO was found to be 25 nm. The lattice parameters calculated from the present data are $a = 4.6890\text{\AA}$, $b = 3.425\text{\AA}$ and $c = 5.1324\text{\AA}$ respectively, which are in good agreement with the reported data (JCPDS no.80-1917). From X-ray diffractogram of the CeO $_2$ -CuO nanocomposite average crystallite size was found to be 10 nm. Decrease in crystallite size of composite as compare to pure nanoparticles shows formation of CeO $_2$ -CuO nanocomposite.

Scanning Electron Microscopy (SEM)

Figure 2.1, 2.2 and 2.3 shows SEM micrographs of the CeO $_2$, CuO nanoparticles and CeO $_2$ -CuO nanocomposite respectively, synthesized by microwave assisted sol-gel method. Homogeneous microstructures were observed for all the materials consisting of crystallites having various size and forms. The content has a great influence on the morphology and structure of the catalysts. The crystal grain size estimated from SEM micrographs was found to be $30\text{ }\mu\text{m}$ for CeO $_2$ and CuO nanoparticles. While for CeO $_2$ -CuO nanocomposite size comes out to be $10\text{ }\mu\text{m}$. This variation in particle size strengthens with XRD analysis. It is clear from Fig. 2.1 that the CeO $_2$ formed is rich in the pores, which is composed of the CeO $_2$ crystallites [29]. It presents that particles are spherical in shape with a uniform size distribution. SEM image of CuO nanoparticles in Fig. 2.2 composed of small bulk particles. The CeO $_2$ -CuO nanocomposite displays spongy-like features with large voids and small spherical agglomerates of CuO, as can be seen from SEM image shown in Fig. 2.3. These structures provide a large surface area and increase the electron transport. Such change in morphology creates voids and windows to generate wide porosity. The surface voids are formed due to the release of excessive volumes of gases upon the combustion reaction, introducing porosity to the prepared CeO $_2$ -CuO nanocomposite materials, which results in reduction in the size of structural features [30]. Accordingly, we can observe the porosity of the samples increases from Fig. 2.1 to 2.3. However, such porous structure is useful in gas sensor application [31].

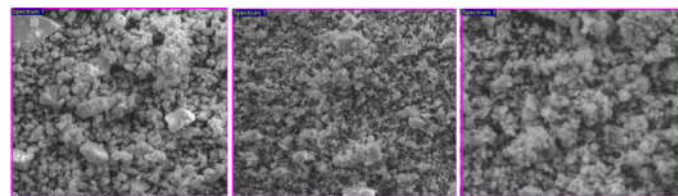
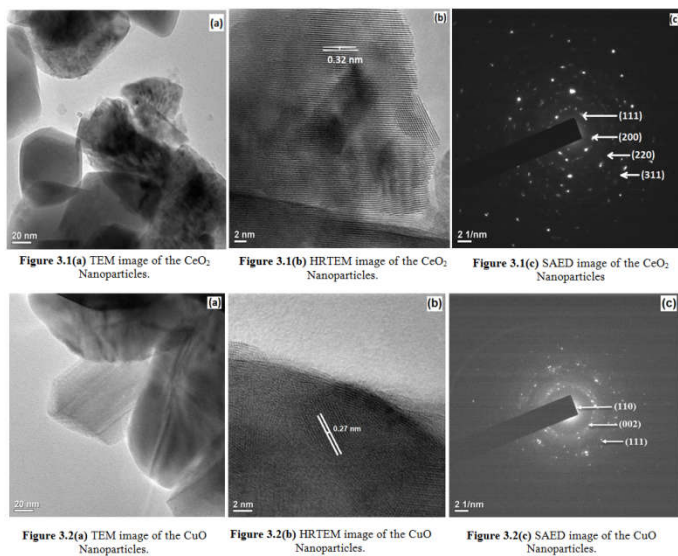


Figure 2.1 SEM image of the CeO $_2$ Nanoparticles. **Figure 2.2** SEM image of the CuO Nanoparticles. **Figure 2.3** SEM image of the CeO $_2$ -CuO Nanocomposite.

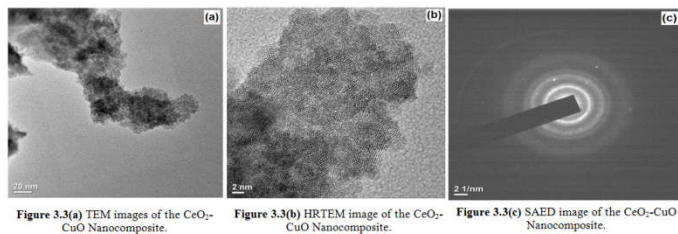
Transmission Electron Microscopic (TEM) analysis

TEM analysis gives information about size and morphology of CeO $_2$, CuO and CeO $_2$ -CuO nanocomposite. The particle size of pure CeO $_2$ and pure CuO samples Fig.

3.1(a) and Fig. 3.2(a) are in the range of 20-30 nm, while for CeO₂-CuO nanocomposite Fig. 3.3(a) the particle size is 5-10 nm. TEM image of CeO₂ particles Fig. 3.1(a) show spherical morphology. The HRTEM image Fig. 3.1(b) shows lattice fringes which allows for identification of crystallographic spacing of CeO₂. It shows horizontal fringes. The fringe $d = 0.32$ nm matches with plane (111) of cubic CeO₂. The HRTEM image of CuO Fig. 3.2(b) shows lattice fringe $d = 0.27$ nm, which corresponds to (110) plane of monoclinic CuO. The TEM image of CeO₂-CuO nanocomposite Fig. 3.3(a) indicates that nanoparticles of CeO₂-CuO are well dispersed with smooth surface of uniform size and shows a homogenous particle distribution. Particles of two types are clearly shown in CeO₂-CuO nanocomposite. From HRTEM image Fig. 3.3(b), it implies that copper may be embedded in the lattice of ceria which can produce oxygen vacancies.



Transmission Electron Microscopic (TEM) analysis



The selected area electron diffraction (SAED) pattern of CeO₂ nanoparticles, CuO nanoparticles and CeO₂-CuO nanocomposite showing in Fig. 3.1(c), 3.2(c), 3.3(c) respectively, discloses polymorphic distinct rings of the crystalline materials. High degree of crystallinity in polycrystals is confirmed from brightness of ring patterns of all samples. The SAED pattern confirms that nanoparticles are polycrystalline in nature. The SAED pattern in the Fig. 3.1(c) and Fig. 3.2(c), also supports the d values obtained from XRD with rings which can be assigned to (111), (200), (220) and (311) planes of CeO₂ structure and (110), (002), (111) planes of CuO structure. The crystalline phases of TEM are in good agreement with XRD data.

UV-Visible

UV-Visible technique was used to identify the absorption range and band gap energy of the composite material. The UV-Visible spectra of CeO₂, CuO nanoparticles and CeO₂-CuO nanocomposite is shown in Fig. 4.1. In pure samples absorption first increases in the ultraviolet region, then there is slow decrease in the ultraviolet region and then fast decreases in visible region. While in composite absorption first decreases, then slowly increases in ultraviolet region and then fast decreases in visible region. Pure CeO₂ gives three absorption peaks at 226 nm, 280 nm and 345 nm, respectively corresponding to O²⁻ → Ce³⁺ and O²⁻ → Ce⁴⁺ charge transfer transactions and inter bands appeared in CeO₂. Simultaneously, pure CuO shows a wide absorption peak at about 380 nm [29]. For CeO₂-CuO composite absorption bands appeared at 224 nm, 268 nm and 274 nm i.e. at lower wavelength as compared to pure oxides. From the absorption data, the band gap energy (E_g) of the material has been calculated using Tauc's equation:

$$\alpha h\nu = A (h\nu - E_g)^n \quad \text{---eq. (2)}$$

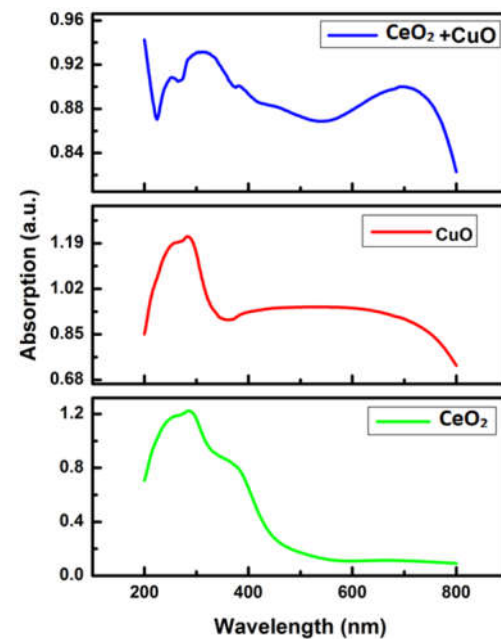


Figure 4.1 UV-Visible Spectra of CeO₂, CuO Nanoparticles and CeO₂-CuO Nanocomposite.

where α is the absorption coefficient and A is constant, $h\nu$ is the photon energy, E_g is the optical band gap of the thin film. "n" is a number which characterizes the mechanism of a transition process, $n = 1/2, 3/2$ for direct transitions and 1, 2, 3 for indirect transitions. The Tauc's plot was used for calculating the value of the direct optical band gap by extrapolating curve to zero absorption as shown in Fig. 4.2. The calculated value of band gap for CeO₂, CuO nanoparticles and CeO₂-CuO composite were found to be 3.19 eV, 1.7 eV and 1.3 eV respectively. The CeO₂-CuO composite shows very low band gap as compared to other materials. This reduction may be caused as results of additional sub-bandgap energy levels are induced with aid of abundant surface and interface defects

within the nanoparticle formation [32]. Thus, the prepared film has a semiconducting nature.

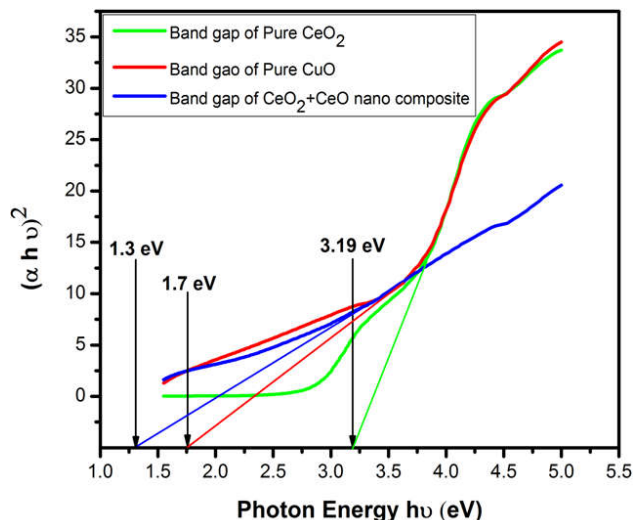


Figure 4.2 Tauc's plot of the CeO₂-CuO Nanocomposite showing the optical energy band gap.

Gas sensing properties

It is well known that CeO₂ as well as CuO are two important kinds of fundamental materials and they have been broadly used as gas sensors. Furthermore, combining two materials will form heterojunction at the intergrain boundaries, which modifies the electronic transport. Hence, it is necessary to study the sensing properties of CeO₂-CuO gas sensor. The gas sensing characteristics of the CeO₂-CuO thin film have been investigated and the results are shown in here. Sensing parameters like sensitivity, percentage of sensor response, response and recovery time have been calculated from the sensing behaviour of the CeO₂-CuO thin film. The gas sensor sensitivity was defined as the ratio of the current through the sample in air containing propane-butane mixture (LPG) at desired concentration to the current value in pure air atmosphere (I_{LPG} / I_{air}). In this case, at constant environmental conditions the value of the current through the sample changes significantly. The measurements were performed in the temperature range from 225°C to 325°C with 25°C step. The gas sensor tests have shown that an increase in propane-butane concentration leads to an increase in the current value. After the gas mixture introduction, the current dependencies have very similar character for all of the samples. It is necessary to point out, that the current value stabilizes after about 10 min. Figure 5.1 shows plot of sensitivity vs LPG concentration (in ppm) for different samples (CeO₂, CuO and CeO₂-CuO) at their operating temperature. Sensitivity is calculated by using following equation [33];

$$\text{Sensitivity} = R_a / R_g \text{--- eq. (3)}$$

where R_a stands for the resistance of gas sensors in the reference gas (usually the air) and R_g stands for the resistance in the reference gas containing target gases. It is found that the sensitivity of the sensor increases as the concentration of LPG increases.

Gas sensing properties

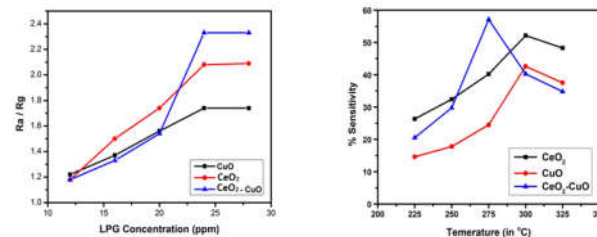
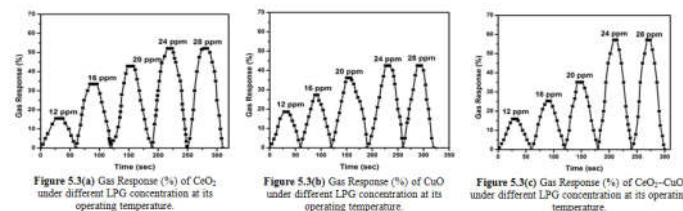


Figure 5.1 Plot of Sensitivity vs LPG concentration (in ppm) for different samples (CeO₂, CuO, CeO₂-CuO) at their operating temperature. Figure 5.2 Plot of % Sensitivity as a function of operating Temperature (in degree Celsius) for different samples (CeO₂, CuO & CeO₂-CuO) for LPG Gas at 24 ppm.



At 24 ppm of LPG concentration all samples show maximum sensitivity. After that, though the concentration of LPG increases sensitivity remains constant. The CeO₂-CuO sensor shows maximum sensitivity as compared to pure samples. It is 2.08, 1.74, and 2.33 for CeO₂, CuO and CeO₂-CuO sensor respectively. Figure 5.2 shows plot of sensitivity as a function of operating temperature (in degree Celsius) for different samples (CeO₂, CuO & CeO₂-CuO) for LPG at 24 ppm. The temperature of the sensor surface is one of the most influencing parameter. The optimum operating temperature for an effective sensor performance corresponds to that where the material is able to catalytically reduce or oxidize the target gas, simultaneously changing the electrical properties of the sensor material [34, 35]. In order to obtain the optimum operating temperature, the samples were exposed to 24 ppm LPG under different temperatures with the interval of 25°C. It is evident from figure that, percentage sensitivity increases at first and reaches its maximum value at the optimum temperature, then decrease with increase in temperature. Such behaviour can be explained by the kinetics and mechanics of gas reaction which occurred on the surface [36]. For low temperatures, the sensor response is confined by the speed of chemical reactions. For higher temperature, the sensor response is confined by the speed of the diffusion of gas molecules to that surface. Operating temperature for CeO₂ and CuO is 300°C, while for CeO₂-CuO it is 275°C. It reveals that, the CeO₂-CuO sensor is more sensitive to LPG at lower operating temperature (275°C) than pure ones. If to order the samples according to their gas sensor sensitivity, we obtain: CuO/CeO₂/CeO₂-CuO. The result is quite sure from their morphology. The highest response has the sample CeO₂-CuO that consists of small spherical agglomerates of CuO and has the largest value of the surface area to the volume ratio [26]. Gas Response (%) of CeO₂, CuO and CeO₂-CuO under different LPG concentration at its operating temperature is shown in Figure 5.3(a), 5.3(b) and 5.3(c) respectively. The resistance of the sensing film increased with respect to time on the exposure to LPG. Next, the sensing element reached a constant value (resistance) and then decreased due to the removal of LPG (recovery characteristics) from

the gas chamber. Also, the sensing curves of the sensor are very broadening due to the increase of LPG concentration. At low concentration, only few gas molecules would adsorb and it covers small area. However, on increasing the concentration, more number of gas molecules and oxygen species would adsorb at the surface of the sensing element, it covers large area of the material. Therefore, the sensitivity of the sensor was increased. It is shown that sensitivity of the CeO₂ based LPG sensors are linearly proportional to their specific surface area [36]. This process involves surface adsorption and reaction of reducing gases. The percentage of the sensor is given by following equation [33];

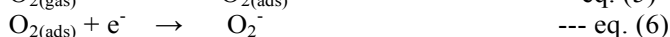
$$\text{Percentage of sensor response} = [R_a - R_g] / R_a * 100 \quad \text{--- eq. (4)}$$

The sensitivity and percentage of the sensor response increased gradually with respect to the concentration of LPG. The maximum percentage of the sensor response was found to be 57.09% at 24 ppm of LPG for CeO₂-CuO, which is the highest response. For CeO₂ and CuO the percentage of the sensor response was 52.13% and 42.59% respectively. Moreover, the sensing curve has repeatability. Because ambient temperature and environmental conditions remain constant. Repeatability is defined as

Table 1 Literature survey on LPG sensing performance of CeO₂-CuO Nanocomposite with reported materials

Sr. No.	Material	Temperature °C	Sensitivity	Concentration ppm	References
1	SnO ₂ -Cu	264	0.79	500	37
2	Al-Ni-SnO ₂	300	16	600	38
3	SnO ₂	274	0.51	500	32
4	ZnO-Cu	500	0.9	400	39
5	CeO ₂ -CuO	275	2.33	24	Present work

The sensing element has ability to produce the same response for successive measurement and it is related to precision. Also, the repeatability reveals that the material permits an efficient and reliable LPG sensor. However, the LPG get fast adsorbed and diffused inside the sensing element. In the recovery sense, the gas desorbed gradually at room temperature and it took long time to recover. The sensing mechanism is based on the adsorption and desorption process at the surface of the sensing film [37, 38]. The environmental oxygen species adsorb on the surface of the CeO₂-CuO thin film. Then, takes out electron from the conduction band to form O⁻ species that increases the resistance of the film. The reaction can be explained by the following equation,



The chemisorbed oxygen reacts with LPG molecules. The above reaction would remove the adsorbed oxygen and then form gaseous species and water vapour. Also, the resistance of the film was changed. The following reaction has occurred between hydrocarbon and chemisorbed oxygen,



where C_nH_{2n+2} represents hydrocarbon. While LPG reacts with surface oxygen, the ignitable items exist, for example, water and potential barrier to charge transport must be created. The development of the potential barrier is expected to decrease the concentration of charge carriers (conduction). Thus increases the resistance of the film with time. In this way, the gas atoms were stopped and afterward oxygen in air would adsorb on the surface of the film (catch of electron). Thus decreases the resistance of the sensing film [32]. Table 1 shows a recent literature survey on LPG sensing performances of pure and composites. From this table, the prepared thin film sensor shows the high sensitivity and response. The results cited in Table 1 and the present work propose that nanocomposites are good candidates for gas sensors with high sensitivity and optimum temperature. Thus, the distinctive feature of our sample, in comparison to different LPG sensors reviewed in the literature is the absence of the characteristic maximum on the sensitivity versus temperature dependencies [39-42].

Response and Recovery time

The Response / Recovery time is an important parameter used for characterizing gas sensors. The time taken for the sensor to attain 90% of maximum change in resistance on exposure to the gas is the response time and the time taken by the sensor to get back 90% of original resistance is the recovery time. Figure 5.4 shows variations in LPG (24 ppm) response with time at temperature 275°C for CeO₂-CuO. The response was quick (~ 25 s) while the recovery time was (~ 50 s). The quick response may be due to faster oxidation of gas.

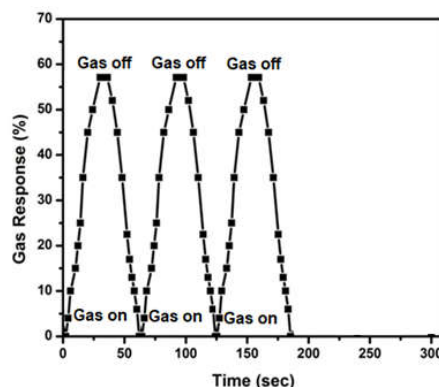


Figure 5.4 Response and Recovery time of CeO₂-CuO Nanocomposite

CONCLUSION

The experimental results showed that the CeO₂-CuO sensing film exhibited high sensitivity for the detection of LPG and the sensitivity depended on the composition of the composites, operating temperature etc. The larger surface area gives more response to react with the target gas. The film seems to be highly porous for oxygen adsorption. Also CuO isolates at the grain boundaries. The isolation of CuO around the boundary of CeO₂ forms a heterojunction between CeO₂ (n) and CuO (p), facilitating the efficient

charge transfer, which enhances sensitivity [43]. The results revealed that, for LPG, the sensitivity of the CeO₂-CuO sensor is 2.33 at 275°C and it was higher than the pure ones. In addition, the dynamical gas sensor response at different temperature values and dependencies of the sensor sensitivity on the temperature at different LPG concentrations in air has been investigated. It has been found that sensor response depends on the sample morphology. If to order the samples according to their gas sensor sensitivity, we obtain: CuO/CeO₂/CeO₂-CuO. The maximum percentage of the sensor response was found to be 57.09% at 24 ppm of LPG for CeO₂-CuO, which is the highest response. The result is quite probable from their morphology. The highest response has the sample CeO₂-CuO that consists of small spherical agglomerates of CuO and has the largest value of the surface area to the volume ratio. It seems that both adsorption and combustion of the reducing gases occur on the surface of the sensors. The depletion of the lattice oxygen might be responsible for the sensitivity of the sensor to the gas.

Acknowledgements

Authors are thankful to SAIF-NEHU, Shillong for providing TEM Facility.

References

- 1 B.S. Shirke, A.A. Patil, P.P. Hankare and K.M. Garadkar, "Synthesis of cerium oxide nanoparticles by microwave technique using propylene glycol as a stabilizing agent," *J. Material Science: Material in Electronics*, Vol. 22, No. 2, 2011, pp. 200-203.
- 2 B.S. Shirke, P.V. Korake, P.P. Hankare, S.R. Bamane and K.M. Garadkar, "Synthesis and characterization of pure anatase TiO₂ nanoparticles," *J. Material Science: Material in Electronics*, Vol. 22, No. 7, 2011, pp. 821-824.
- 3 L.A. Ghule, B.S. Shirke, K.B. Sapnar, S.D. Dhole, P.P. Hankare and K.M. Garadkar, "Preparation of zinc oxide nanorods by microwave assisted technique using ethylene glycol as a stabilizing agent," *J. Material Science: Material in Electronics*, Vol. 22, No. 8, 2011, pp. 1120-1123.
- 4 M. N. Nadagouda, T. F. Speth and R. S. Varma, "Microwave-assisted Green Synthesis of Silver Nanostructures," *Acc Chem Res*, Vol. 44, No. 7, 2011, pp. 469-478.
- 5 K. M. Garadkar, A. N. Kadam and Jinsub Park, "Microwave-assisted sol-gel synthesis of metal oxide nanomaterials," *L. Klein., Handbook of Sol-Gel Science and Technology*, part of Springer Nature, 2018, pp. 483-504, DOI: 10.1007/978-3-319-32101-1_107.
- 6 M.Y. Cui, X.Q. Yao, W.J. Dong, K. Tsukamoto, C.R. Li, "Template-free synthesis of CuO-CeO₂ nanowires by hydrothermal technology," *Journal of Crystal Growth*, Vol. 312, No. 2, 2010, pp. 287-293.
- 7 Cristhiane Guimaraes Maciel, Tatiana de Freitas Silva, Marcelo Iuki Hirooka, Mohamed Naceur Belgacem and Jose Mansur Assaf, "Effect of nature of ceria support in CuO/CeO₂ catalyst for PROX-CO reaction," *Fuel*, Vol. 97, 2012, pp. 245-252.
- 8 Ashwani Sharma, Pallavi, Sanjay Kumar and Sonia, "Synthesis and Characterization of CeO-CuO Nanocomposites," *Archives of Applied Science Research*, Vol. 4, No. 6, 2012, 2557-2563.
- 9 Chengxiang Wang, Longwei Yin, Luyuan Zhang, Dong Xiang and Rui Gao, "Metal Oxide Gas Sensors: Sensitivity and Influencing Factors," *Sensors*, Vol. 10, 2010, pp. 2088-2106.
- 10 Feng Zhao, Shuangde Li, Xiaofeng Wu, Renliang Yue, Weiman Li, Xicuo Zha, Yuzhou Deng and Yunfa Chen, "Catalytic Behaviour of Flame-Made CuO-CeO₂ Nanocatalysts in Efficient CO Oxidation," *Catalysts*, Vol. 9, 2019, pp. 256-273. doi:10.3390/catal9030256
- 11 G. Sedmak, S. Hočevár and J. Levec, "Kinetics of selective CO oxidation in excess of H₂ over the nanostructured CuO," *Journal of Catalysis*, Vol. 213, No. 2, 2003, pp. 135-150.
- 12 Konsolakis, M., "The role of Copper-Ceria interactions in catalysis science: Recent theoretical and experimental advance," *Appl. Catal. B Environ*, Vol. 198, 2016, pp. 49-66.
- 13 Sun S, Mao D, Yu J, Yang Z, Lu G, Ma Z. "Low-temperature CO oxidation on CuO/CeO₂ catalysts: The significant effect of copper precursor and calcination temperature," *Catalysis Science & Technology*, Vol. 5, No. 6, 2015, pp. 3166-3181.
- 14 Lin L., Yao S., Liu Z., Zhang F., Li N., Vovchok D., Martínez-Arias A., Castañeda R., Lin J., Senanayake S.D., "Characterization of Cu/CeO₂ Nanocatalysts for CO₂ Hydrogenation: Morphological Effects of Nanostructured Ceria on the Catalytic Activity," *J. Phys. Chem. C*, Vol. 122, 2018, pp. 12934-12943. doi: 10.1021/acs.jpcc.8b03596.
- 15 Chen C., Zhan Y., Zhou J., Li D., Zhang Y., Lin X., Jiang L., Zheng Q., "Cu/CeO₂ Catalyst for Water-Gas Shift Reaction: Effect of CeO₂ Pretreatment," *Chem Phys Chem*, Vol. 19, 2018, pp. 1448.
- 16 Barbato P.S., Colussi S., Di Benedetto A., Landi G., Lisi L., Llorca J., Trovarelli A., "Origin of High Activity and Selectivity of CuO/CeO₂ Catalysts Prepared by Solution Combustion Synthesis in CO-PROX Reaction," *J. Phys. Chem. C*, Vol. 120, No. 24, 2016, pp. 13039-13048.
- 17 Sudarsanam P., Hillary B., Malleshm B., Rao B.G., Amin M.H., Nafady A., Alsalmé A.M., Reddy B.M., Bhargava S.K., "Designing CuOx Nanoparticle-Decorated CeO₂ Nanocubes for Catalytic Soot Oxidation: Role of the Nanointerface in the Catalytic Performance of Heterostructured Nanomaterials," *Langmuir*, Vol. 32, No. 9, 2016, pp. 2208-2215.
- 18 Dongsong Zhang, Xianjun Du, Liyi Shi, Ruihua Gao, "Shape-controlled synthesis and catalytic application of ceria nanomaterials," *Dalton Trans*, Vol. 41, 2012, pp. 14455-14475.
- 19 Z. Wang, Z. Quan, J. Lin, "Remarkable Changes in the Optical Properties of CeO₂ Nanocrystals Induced by Lanthanide Ions Doping," *Inorg. Chem*, Vol. 46, No. 13, 2007, pp. 5237-5242.
- 20 Z. K. Ghouri, N.A.M. Barakat, Al-Mahmudur Alam, Mira Park, Tae Hwan Han, Hak Yong Kim, "Facile synthesis of Fe/CeO₂-doped CNFs and Their

- Capacitance Behavior," *Int. J. Electrochem. Sci.*, Vol. 10, 2015, pp. 2064-2071.
- 21 Wang J., Pu H., Wan G., Chen K., Lu J., Lei Y., Zhong L., He S., Han C., Luo Y., "Promoted the reduction of Cu²⁺ to enhance CuO-CeO₂ catalysts for CO preferential oxidation in H₂-rich streams: Effects of preparation methods and copper precursors," *Int. J. Hydrogen Energy*, Vol. 42, No. 34, 2017, pp. 21955-21968.
- 22 Shang, H. Zhang, X. Xu, J. Han, "Effects of preparation methods on the activity of CuO/CeO₂ catalysts for CO oxidation," *Front. Chem. Sci. Eng.*, Vol. 11, 2017, pp. 603-612.
- 23 Xiaoxin Li, Xiaogan Li, Ning Chen, Xinye Li, Jianwei Zhang, Jun Yu, Jing Wang, and Zhenan Tang, "CuO-In₂O₃ Core-Shell Nanowire Based Chemical Gas Sensors," *Hindawi Publishing Corporation Journal of Nanomaterials*, Volume 2014, Article ID 973156, 7 pages.
- 24 K.R. Nemade, S.A. Waghuley, "LPG sensing performance of CuO-Ag₂O bimetallic oxide nanoparticles," *St. Petersburg Polytechnical University Journal: Physics and Mathematics*, Vol. 1, No. 3, 2015, pp. 249-255.
- 25 E. Jebamalar Leavline, D. Asir Antony Gnana Singh, B. Abinaya and H. Deepika, "LPG Gas Leakage Detection and Alert System," *International Journal of Electronics Engineering Research*, Vol. 9, No. 7, 2017, pp. 1095-1097.
- 26 V.M. Latyshev, T.O. Berestok, A.S. Opanasyuk, A.S. Korniyushchenko, V.I. Perekrestov, "Nanostructured ZnO films for potential use in LPG gas sensors," *Solid State Sciences*, Vol. 67, 2017, pp. 109-113.
- 27 Saranyoo Chaiwichian, Burapat Inceesungvorn, kanlaya Pingmuang, khatcharin Wetchakun, Sukon Phanichphant, Natda Wetchakun, "Synthesis and Characterization of the Novel BiVO₄/CeO₂ Nanocomposites," *Engineering Journal*, Vol. 16, No. 3, 2012, pp. 153-160.
- 28 Chivukula Srikanth, Chakradhar Sridhar, B.M. Nagabhushana, and R.D. Mathad, "Characterization and DC Conductivity of Novel CuO doped Polyvinyl Alcohol (PVA) Nanocomposite Films," *Int. Journal of Engineering Research and Applications*, Vol. 4, No. 10, 2014, pp. 38-46.
- 29 Shanghong Zeng, Yan Wang, Suping Ding, Jesper J.H.B. Sattler, Elena Borodina, Lu Zhang, Bert M. Weckhuysen, Haiquan Su, "Active sites over CuO/CeO₂ and inverse CeO₂/CuO catalysts for preferential CO oxidation," *Journal of Power Sources*, Vol. 256, 2014, pp. 301-311.
- 30 Abdallahthe F. Zedan, and Amina S. Al Jaber, "Combustion Synthesis of Non-Precious CuO-CeO₂ Nanocrystalline Catalysts with Enhanced Catalytic Activity for Methane Oxidation," *Materials*, Vol. 12, No. 6, 2019, 878; doi:10.3390/ma12060878.
- 31 A. K. Sharma, S. S. Potdar, K. S. Pakhare, B. M. Sargar, M. V. Rokade, N. L. Tarwal, "The selective ethanol gas sensing performance of CdO₁-xZnOx nanocomposite," *J Mater Sci: Mater Electron*, doi:10.1007/s10854-016-5984-1.
- 32 V. Manikandan, Monika Singh, B.C. Yadav, Juliano C. Denardin, "Fabrication of lithium substituted copper ferrite (Li-CuFe₂O₄) thin film as an efficient gas sensor at room temperature," *Journal of Science: Advanced Materials and Devices*, Vol. 3, No. 2, 2018, pp. 145-150.
- 33 M. Singh, B.C. Yadav, A. Ranjan, R.K. Sonker, M. Kaur, "Detection of liquefied petroleum gas below lowest explosion limit (LEL) using nanostructured hexagonal strontium ferrite thin film," *Sens. Actuators B Chem*, Vol. 249, 2017, pp. 96-104.
- 34 K.M. Garadkar, B.S. Shirke, Y.B. Patil and D.R. Patil, "Nanostructured ZrO₂ Thick Film Resistors as H₂-Gas Sensors Operable at Room Temperature," *Sensors & Transducers Journal*, Vol. 110, No. 11, 2009, pp. 17.
- 35 K. M. Garadkar, B. S. Shirke, P. P. Hankare and D. R. Patil, "Low cost nanostructured anatase TiO₂ as a H₂S gas sensor synthesized by microwave assisted technique," *Sensor Letters*, Vol. 9, No. 2, 2011, pp. 526-532.
- 36 F. Pourfayaz, A. Khodadadi, Y. Mortazavi, S.S. Mohajerzadeh, "CeO₂ doped SnO₂ sensor selective to ethanol in presence of CO, LPG and CH₄," *sensors and Actuators B Chemical*, Vol. 108, 2005, pp. 172-176.
- 37 B.C. Yadav, S. Singh, A. Yadav, "Nanonails structured ferric oxide thick film as room temperature liquefied petroleum gas (LPG) sensor," *Appl. Surf. Sci.*, Vol. 257, No. 6, 2011, pp. 1960-1966.
- 38 A. Singh, S. Singh, P. Tandon, R.R. Yadav, "Synthesis, Characterization and Gas Sensing Capability of NixCu_{1-x}Fe₂O₄ (0.0 ≤ x ≤ 0.8) Nanostructures Prepared via Sol-Gel Method," *J. Inorg. Organomet. Polym. Mater.*, Vol. 26, 2016, pp. 1392; <https://doi.org/10.1007/s10904-016-0428-1>.
- 39 A. D. Inamdar and R. C. Aiyer, "High performance SnO₂-Cu sensor for LPG and CO," *Asian Journal of Physics*, Vol. 9, No. 1, 2005, pp. 1-8.
- 40 K. Jain, R. P. Pant, S. T. Laxmikumar, "Effect of Ni Doping on Thick Film SnO₂ Gas Sensor," *Sensors and Actuators B: Chemical*, Vol. 113, No. 2, 2006, pp. 823-829.
- 41 Shrivastava A, Rashmi, Jain K, "Study on ZnO-doped tin oxide thick film gas sensors. *Materials Chemistry and Physics*," Vol. 105, No. (2-3): 2007, pp. 385-390.
- 42 Raju A R, Rao C N., "Gas-sensing characteristics of ZnO and copper-impregnated ZnO," *Sensors and Actuators B: Chemical*, Vol. 3, No. 4, 1991, pp. 305-310.
- 43 Madhavrao K. Deore, Vishwas B. Gaikwad and Gotan H. Jain, "Role of CuO-ZnO heterojunctions in gas sensing response of CuO-ZnO thick films," *Journal of Physical Science and Application, International*, Vol. 6, No. 2, 2016, pp. 51-60.
